Int. J. Multiphase Flow Vol. 15, No. 6, pp. 857–875, 1989
Printed in Great Britain.

0301-9322/89 $3.00 + 0.00

PRESSURE WAVES IN SATURATED POROUS MEDIA

V. E. NAKORYAKOV, V. V. KUZNETSOV and V. E. DONTSOV
Institute of Thermophysics of the Siberian Branch of the U.S.S.R., Academy of Sciences, Novosibirsk-90, 630090, U.S.S.R.

(*Received* 30 *April* 1987; *in revised form* 25 *December* 1988)

Abstract—The evolution and structure of pressure perturbations in a liquid-saturated porous medium and liquid-saturated porous media with gas bubbles has been investigated experimentally. The existence of two types of longitudinal pressure waves in consolidated porous media has been confirmed. The set of equations which describes the propagation of pressure waves of finite amplitude in an elastic gas bubble liquid-saturated porous medium was obtained. The pressure wave evolution in saturated porous media has been calculated by the Biot model and a good correlation with the experiment was obtained.

Key Words: liquid-saturated porous media, pressure waves, gas bubbles, wave structures

1. INTRODUCTION

Theoretical analyses of pressure wave propagation in liquid-saturated porous media, given in the works by Biot (1956), Nikolayevsky *et al.* (1970) and Nigmatulin (1978), have shown that interphase friction on the fluid–rigid skeleton interface is the basic mechanism of wave evolution. Lyakhov (1974), Domenico (1977), Hovem & Ingram (1979) and Salin & Schon (1981) have shown that in unconsolidated porous media one longitudinal wave propagates, whose velocity is determined basically by the bulk modulus of the liquid. A comparison between experimental data on high-frequency acoustic wave attenuation and calculations using Biot's (1956) model shows a considerable discrepancy between the experimental data and calculation. In the region of high frequencies Salin & Schon (1981) account for this discrepancy by the effect of high-frequency scattering on the skeleton grains. For low frequencies, McCann & McCann (1985) have shown recently that taking into account the pore size distribution in a modified Biot model allows us to generalize the experimental data better. For the first time Plona (1980) and Johnson & Plona (1982) have experimentally revealed for ultrasonic waves in a consolidated liquid-saturated porous medium the existence of two types of longtitudinal waves, a "quick" one and a "slow" one, caused by the different compressibilities of the liquid phase and rigid skeleton.

The existence of gas bubbles in liquid-saturated porous media sufficiently decreases the compressibility of the liquid phase, leading to the decrease in the "quick" wave and "slow" wave velocities and to the increase in amplitude attenuation. Nikolayevsky *et al.* (1970) have theoretically studied the pressure wave propagation in a gas bubble liquid-saturated porous medium assuming equality of the gas and liquid pressure. A linear set of equations for three-phase mixtures (porous skeleton, liquid, gas bubbles) with bubble dynamics was obtained by Bedford & Stern (1983) with the help of the Hamilton variational principle. Taking into account gas bubble dynamics, they calculated the phase velocity and harmonic wave attenuation vs frequency in an unconsolidated porous medium. Anderson & Hampton (1980) presented experimental data on the acoustic rigidity of a three-phase medium vs frequency, which proves the importance of gas bubble dynamics in acoustic waves.

In this paper experimental data are presented on pressure wave structure and dynamics in liquid-saturated and gas bubble liquid-saturated porous media for a wide range of wave and medium parameters. The data were correlated with the help of known theoretical models, and the set of equations which describes the propagation of one-dimensional pressure perturbations of finite amplitude in an elastic porous medium saturated by liquid with gas bubbles was obtained.

2. THEORETICAL ANALYSIS AND NUMERICAL CALCULATIONS

Let us analyse the propagation of one-dimensional pressure perturbations in a liquid-saturated porous medium containing elastic gas bubbles, assuming that the perturbation wavelength is much greater than the interbubble distance. According to visual observations and the data of Wardlaw & Kellar (1985), at small void fractions the gas phase is, as a rule, in the form of bubbles occupying not more than one pore size. This allows us to consider a gas bubble liquid as a homogeneous mixture with mean density ρ_m, mean pressure p_m and mean velocity v_m. To describe one-dimensional pressure perturbations in a porous medium saturated with such a homogeneous mixture, we use the model of multivelocity continuum for a porous medium saturated with an effective liquid (Nigmatulin 1978). The following assumptions are made:

1. The size of inhomogeneities in a multiphase medium is essentially larger than molecular kinetic sizes.
2. Phase transitions are absent.
3. Microdeformations of the solid phase and variations of its real density are small.
4. The kinetic energy of pulsative motion and pulsative momentum transfer are small, not only in the solid phase but in the liquid one as well.
5. The averaged tensor of viscous stresses in a liquid is small and the liquid viscosity will be taken into account only in a force of interphase interaction.

The mass and momentum conservation equations of the solid and liquid phases, which are averaged with respect to volume, incorporate the pressure gradients in the liquid and fictitious stresses in a solid skeleton, as well as interphase forces related to viscous forces on an interphase surface and small-scale pressure pulsations due to acceleration of phases relative to each other. Nigmatulin (1978) obtained expressions for the components of interphase force due to viscosity F_μ at small Re. This force is of the form

$$F_\mu = \frac{\phi^2 \nu \rho_2}{K_0}(v_2 - v_1)$$

with small-scale inertial effects

$$F_m = \aleph \phi (1-\phi)\rho_2 \frac{d(v_2 - v_1)}{dt} \quad \aleph = \frac{(\alpha - 1)}{(1-\phi)}$$

and the first component of the tensor for the fictitious stresses in a solid skeleton

$$\sigma^f = (K_B + \tfrac{4}{3}\mu)e_1 + \frac{K_B p_m}{K_1}.$$

Taking into account these correlations, a system of equations describing the propagation of one-dimensional pressure perturbations in the frame of a multivelocity continuum (Nigmatulin 1978) can be written as follows:

$$\frac{\partial \phi \rho_m}{\partial t} + \frac{\partial \phi \rho_m v_m}{\partial x} = 0, \tag{1}$$

$$\frac{\partial (1-\phi)\rho_1}{\partial t} + \frac{\partial (1-\phi)\rho_1 v_1}{\partial x} = 0, \tag{2}$$

$$\alpha \phi \rho_m \frac{dv_m}{dt} - (\alpha - 1)\phi \rho_m \frac{dv_1}{dt} = -\phi \frac{\partial p_m}{\partial x} - \frac{\phi^2 \nu \rho_m}{K_0}(v_m - v_1), \tag{3}$$

$$-(\alpha - 1)\phi \rho_m \frac{dv_m}{dt} + [(1-\phi)\rho_1 + (\alpha - 1)\phi \rho_m]\frac{dv_1}{dt} = -(1-\phi)\frac{\partial p_m}{\partial x} + \frac{\partial \sigma^f}{\partial x} + \frac{\phi^2 \nu \rho_m}{K_0}(v_m - v_1), \tag{4}$$

$$\sigma^f = (K_B + \tfrac{4}{3}\mu)e_1 + \frac{K_B}{K_1}p_m, \tag{5}$$

$$\frac{\partial e_1}{\partial t} = \frac{\partial v_1}{\partial x}, \tag{6}$$

$$\frac{\rho_1}{\rho_{10}} = 1 + \frac{1}{K_1}\left(p_m - p_0 - \frac{K_B e_1}{1-\phi}\right) \quad [7]$$

and

$$\rho_m = \rho_2(1-\epsilon) + \rho_3\epsilon; \quad [8]$$

here x and t are coordinate and time, respectively; ρ is density; v is velocity; p is pressure; σ^f is the first component of the tensor of the effective stresses in the rigid skeleton; ϕ is porosity; K_0 is the permeability of the medium; α is the coefficient of added liquid mass; e_1 is the rigid skeleton deformation; K_B and μ are the moduli of the volumetric elasticity and porous skeleton shift, respectively; K_1 is the modulus of the volumetric elasticity of the porous skeleton material; ν is the kinematic liquid viscosity; and ϵ is the void fraction in the liquid. The subscripts denote the following: 1—the solid phase; 2—the liquid phase; 3—the gas phase; m—a gas–liquid mixture; 0—the initial phase state.

Equations [1] and [3] represent the mass and momentum conservation for a gas–liquid mixture, with [2] and [4] representing the same for a solid skeleton. Equation [6] follows from determining the velocity and deformation of a rigid skeleton at small deformations. Equation [7] is an equation of the solid phase state.

Following the works by Nakoryakov *et al.* (1972, 1983) let us establish the correspondence between pressure and density in a homogeneous mixture. Assuming the possibility of the substitution of pressure in the liquid far from the bubbles p_∞ instead of pressure in the mixture p_m, we obtain, first, an equation for a single bubble pulsation in a porous medium, which follows from the set of equations of continuity and motion of a noncompressible liquid in a porous skeleton in spherical coordinates relative to the bubble centre with radius R:

$$\frac{\partial v_r}{\partial r} + \frac{2v_r}{r} = 0 \quad [9]$$

and

$$\frac{\partial v_r}{\partial t} + v_r\frac{\partial v_r}{\partial r} = -\frac{1}{\rho_2}\frac{\partial p_2}{\partial r} - \frac{\phi\nu}{K_0}v_r \quad [10]$$

with boundary conditions

$$p_2 = p_\infty, \quad v_r = 0 \quad \text{at} \quad r \to \infty \quad [11]$$

and

$$p_2 = p_3(R) - \frac{4\nu\rho_2}{R}\frac{dR}{dt} - p_c \quad \text{at} \quad r = R, \quad [12]$$

where v_r is the radial liquid velocity near the gas bubbles and p_c is the capillary pressures on a gas–liquid boundary. At small void fractions $\epsilon_0 < 0.1$ the gas bubbles occupy, as a rule, one pore size and $p_c = 2\sigma/R$, where σ is the coefficient of surface tension.

Integrating [9] and [10] with boundary conditions [11] and [12] yields the following system of equations:

$$R\frac{d^2R}{dt^2} + \frac{3}{2}\left(\frac{dR}{dt}\right)^2 + \frac{4\nu}{R}\left(1 + \frac{\phi R^2}{4K_0}\right)\frac{dR}{dt} = \frac{p_3(R) - p_\infty}{\rho_2} - \frac{2\sigma}{R}. \quad [13]$$

For small bubble oscillations $\delta R/R_0 < 1$, and assuming the number of bubbles per unit volume of medium is constant, one can write the relations for the transformation from bubble radius to mixture density in [13] in the following form:

$$\frac{dR}{dt} = -\left(\frac{R_0}{3\rho_{m0}\epsilon_0}\right)\cdot\left(\frac{d\rho_m}{dt} - \frac{1}{c_2^2}\frac{dp_m}{dt}\right) \quad [14]$$

and

$$R\frac{d^2R}{dt^2} = -\left(\frac{R_0^2}{3\rho_{m0}\epsilon_0}\right)\left(\frac{d^2\rho_m}{dt^2} - \frac{1}{c_2^2}\frac{d^2p_m}{dt^2}\right), \quad [15]$$

where c_2 is the speed of sound in the liquid.

Assuming that a bubble is compressed adiabatically, the equation for the gas state in a bubble yields the equation for gas pressure and, to an accuracy of $(\delta\rho/\rho_{m0}\epsilon_0)^2$, we obtain:

$$\delta p_3(R) = p_3(R) - p_0 = c_0^2 \delta\rho_m \left[1 + \frac{(\gamma+1)\delta\rho_m}{2\rho_{m0}\epsilon_0}\left(1 - \frac{1}{c_2^2}\frac{\partial p_m}{\partial \rho_m}\right)\right] \quad [16]$$

and

$$c_0 = \left[\frac{\rho_{m0}\epsilon_0}{\gamma p_0} + \frac{(1-\epsilon_0)^2}{c_2^2}\right]^{-1/2}, \quad [17]$$

where $\delta\rho_m = \rho_m - \rho_{m0}$, c_0 is the low-frequency speed of sound in the gas–liquid mixture with allowance for the liquid compressibility and γ is the adiabatic index.

Taking into account [14]–[16], [13] has the form:

$$\delta p_m = p_m - p_0 = \left[1 + \frac{2\sigma}{\rho_0 R_0}\frac{\epsilon_0}{3\gamma_0} + \left(1 - \frac{1}{c_2^2}\frac{\partial p_m}{\partial \rho_m}\right)B\delta\rho_m\right]c_0^2\delta\rho_m$$
$$+ \beta\left(\frac{\partial^2\rho_m}{\partial t^2} - \frac{1}{c_2^2}\frac{\partial^2\rho_m}{\partial t^2}\right) + \frac{4\nu^*}{3\epsilon_0}\left(\frac{\partial\rho_m}{\partial t} - \frac{1}{c_2^2}\frac{\partial p_m}{\partial t}\right) + \frac{2\sigma}{R_0}, \quad [18]$$

where $B = (\gamma+1)/(2\rho_{m0}\epsilon_0)$ is the nonlinearity coefficient,

$$\beta = \frac{R_0^2}{3\epsilon_0}$$

is the dispersion coefficient and

$$\nu^* = \nu\left(1 + \frac{\phi R_0^2}{4K_0}\right).$$

For bubbles with radius $> 10\ \mu$m capillary forces yield corrections to terms in [17] not more than 1%, and so they are not taken into account.

It was shown in the works by Nakoryakov *et al.* (1972, 1983) that for a liquid with gas bubbles the nonlinearity caused by the equation of the gas state is much greater than the hydrodynamic nonlinearity. This allows linearization of the set of equations [1]–[8] for waves of finite amplitude and its reduction into the set of equations for p_m, σ^f, ρ_m:

$$\rho_{m0}\left(M - \frac{\alpha C}{\phi}\right)\frac{\partial^2\sigma^f}{\partial t^2} - \rho_{m0}\left[M - C + \frac{\alpha(H-C)}{\phi}\right]\frac{\partial^2 p_m}{\partial t^2} + (MH - C^2)\frac{\partial^2 p_m}{\partial x^2}$$
$$- \frac{\nu\rho_{m0}}{K_0}\frac{\partial[C\sigma^f + (H-C)p_m]}{\partial t} = (MH - C^2)\left[\alpha\frac{\partial^2\left(\rho_m - \frac{p_m}{c_0^2}\right)}{\partial t^2} + \frac{\nu}{K_0}\frac{\partial\left(\rho_m - \frac{p_m}{c_0^2}\right)}{\partial t}\right] \quad [19]$$

and

$$(\rho_0 M - \rho_{m0}C)\frac{\partial^2\sigma^f}{\partial t^2} + [\rho_0(M-C) + \rho_{m0}(H-C)]\frac{\partial^2 p_m}{\partial t^2}$$
$$+ (MH - C^2)\frac{\partial^2(p_m - \sigma^f)}{\partial x^2} = (MH - C^2)\phi\frac{\partial^2\left(\rho_m - \frac{p_m}{c_0^2}\right)}{\partial t^2}, \quad [20]$$

where

$$H = K_B + \tfrac{4}{3}\mu + \frac{(K_l - K_B)^2}{D - K_B}, \qquad M = \frac{K_l^2}{D - K_B},$$

$$C = \frac{K_l(K_l - K_B)}{D - K_B}, \qquad D = K_l\left[1 + \phi\left(\frac{K_l}{K_m} - 1\right)\right],$$

$K_m = c_0^2\rho_{m0}$ is the modulus of the bulk elasticity of the gas–liquid mixture and $\rho_0 = \rho_{10}\cdot(1-\phi) + \rho_{m0}\phi$.

The set of equations [18]–[20] forms a closed system which describes the propagation of pressure waves of finite amplitude in an elastic porous medium saturated with liquid containing gas bubbles. Unlike the equations obtained by Bedford & Stern (1983), [18–20] take into account the nonlinearity features caused by the gas bubbles and the viscous attenuation caused by the radial motion of the liquid near oscillating bubbles. This attenuation for low-permeable porous media prevails over thermal and dissipative losses.

For pressure perturbations with typical frequency $\omega < \omega_r$ [$\omega_r = (3\gamma p_0/\rho_{20}R_0^2)^{1/2}$ is the resonant bubble frequency] at small but finite nonlinearity, dispersion and viscosity, it follows from [18] that

$$\delta\rho_m = \frac{\delta p_m}{c_0^2} + 0(\mathscr{E}). \qquad [21]$$

Substitution of [21] into negligible small members of [18] at the first approximation yields:

$$\delta\left(\rho_m - \frac{p_m}{c_0^2}\right) = \frac{1}{c_0^4}\left(1 - \frac{c_2^2}{c_0^2}\right)\left[B(\delta\rho_m)^2 + \frac{4\nu^*}{3\epsilon_0}\frac{\partial p_m}{\partial t} + \beta\frac{\partial^2 p_m}{\partial t^2}\right]. \qquad [22]$$

Excluding with the help of [22] the density of the homogeneous mixture ρ_m in [19] and [20], we obtain the equation set for p_m and σ^f for the evolution of low-frequency pressure waves of finite amplitude in a gas bubble liquid-saturated porous medium.

For waves of small amplitude and typical frequency $\omega \ll \omega_r$, when one can ignore in [19] and [20] nonlinear and dispersion effects and the viscous attenuation due to the radial oscillation of the liquid near bubbles, we obtain a linear set of equations for p_m and σ^f:

$$\rho_{m0}\left(M - \frac{\alpha C}{\phi}\right)\frac{\partial^2\sigma^f}{\partial t^2} - \rho_{m0}\left[M - C + \frac{\alpha(H-C)}{\phi}\right]\frac{\partial^2 p_m}{\partial t^2} + (MH - C^2)\frac{\partial^2 p_m}{\partial x^2} - \frac{\nu\rho_{m0}}{K_0}\frac{\partial[C\sigma^f + (H-C)p_m]}{\partial t} = 0 \qquad [23]$$

and

$$(\rho_0 M - \rho_{m0}C)\frac{\partial^2\sigma^f}{\partial t^2} + [\rho_0(M-C) + \rho_{m0}(H-C)]\frac{\partial^2 p_m}{\partial t^2} + (MH - C^2)\frac{\partial^2(p_m - \sigma^f)}{\partial x^2} = 0. \qquad [24]$$

The system [23, 24] was numerically solved by the method of fast Fourier transform by expansion of initial perturbations into Fourier discrete series and analysis of the propagation of each harmonic by means of a system dispersive relation. By reverse transformation at the necessary distance from the medium input we obtain the wave profile at this point and the wave velocity values. According to Biot (1956), for harmonic waves in a porous medium the interphase friction at the liquids–rigid skeleton interface vs frequency was taken into account by substitution of the viscosity $\bar{\nu}$ for ν into [23, 24]:

$$\bar{\nu} = \nu \cdot F(\omega), \qquad [25]$$

where

$$F(\omega) = \frac{s \cdot T(s)}{4\left(1 - \dfrac{2T(s)}{is}\right)}$$

and

$$T(s) = \frac{\mathrm{Ber}'(s) + i\,\mathrm{Bei}'(s)}{\mathrm{Ber}(s) + i\,\mathrm{Bei}(s)}, \quad s = \left(\frac{\omega}{\omega_c}\right)^{1/2};$$

ω_c are the characteristic frequencies of the porous medium, which for chaotic packing of round spheres are equal to $\omega_c = \phi\nu/20K_0$ (Salin & Schon 1981). The functions Ber and Bei are the real and imaginary parts of the Kelvin function, respectively.

Substituting the solution in the form of

$$p_m = p_n \exp[i(\omega_n t - Kx)] + p_0 \qquad [26]$$

and

$$\sigma^f = \sigma_n \exp[i(\omega_n t - Kx)] \qquad [27]$$

into [23, 24], and taking into account [25], we obtain the wavenumber K vs frequency ω_n:

$$\left(\frac{K_{1,2}}{\omega_n}\right)^2 = \frac{1}{2(MH - C^2)}\left\{\left[\frac{\alpha\rho_{m0}H}{\phi} + \rho_0 M - 2\rho_{m0}C - \frac{iv\rho_{m0}HF(\omega)}{K_0\omega_n}\right]\right.$$

$$\mp \left\{\left[\frac{\alpha\rho_{m0}H}{\phi} + \rho_0 M - 2\rho_{m0}C - \frac{iv\rho_{m0}HF(\omega)}{K_0\omega_n}\right]^2 - 4(MH - C^2)\right.$$

$$\left.\left.\cdot\left[\frac{\alpha\rho_0\rho_{m0}}{\phi} - \rho_{m0}^2 - \frac{iv\rho_0\rho_{m0}F(\omega)}{K_0\omega_n}\right]\right\}^{1/2}\right\}; \qquad [28]$$

and pressure amplitudes $p_{n1,2}$ vs effective stress $\sigma_{n1,2}$,

$$\frac{p_{n1,2}}{\sigma_{n1,2}} = \left[\left(\frac{K_{1,2}}{\omega_n}\right)^2 - \frac{M\rho_0 - C\rho_{m0}}{MH - C^2}\right]\cdot\left[\left(\frac{K_{1,2}}{\omega_n}\right)^2 - \frac{\rho_0(M - C) + \rho_{m0}(H - C)}{MH - C^2}\right]^{-1}. \qquad [29]$$

It follows from [28] that two types of longitudinal waves can propagate in one direction in the porous medium. Subscript 1 (negative sign in [28]) corresponds to the "quick" wave, and subscript 2 corresponds to the "slow" wave according to Biot (1956). Taking this into account, the solution of [23, 24] can be written as:

$$p_m(x, t) = \sum_{n=0}^{L} [p_{n,1} \exp i(\omega_n t - K_1 x) + p_{n,2} \exp i(\omega_n t - K_2 x)] + p_0 \qquad [30]$$

and

$$\sigma^f(x, t) = \sum_{n=0}^{L} [\sigma_{n,1} \exp i(\omega_n t - K_1 x) + \sigma_{n,2} \exp i(\omega_n t - K_2 x)]. \qquad [31]$$

The values $p_{n,1}$, $\sigma_{n,1}$ and $p_{n,2}$, $\sigma_{n,2}$ correspond to the initial amplitudes of the pressure waves and tension with wavenumbers K_1 and K_2, respectively. They are determined from expansion of the initial signal into Fourier discrete series,

$$p_m(0, t) = \sum_{n=0}^{L} (p_{n,1} + p_{n,2}) \exp i\omega_n t + p_0 \qquad [32]$$

and

$$\sigma^f(0, t) = \sum_{n=0}^{L} (\sigma_{n,1} + \sigma_{n,2}) \exp i\omega_n t, \qquad [33]$$

with the use of [29].

The values $p_m(0, t)$ and $\sigma^f(0, t)$ are given by the boundary conditions at the input into the porous medium. According to terminology used by Nikolayevsky *et al.* (1970), the boundary condition "liquid piston" (i.e. the pressure in the liquid and the effective tension on the interface) is

$$p_m(0, t) - p_0 = \Delta p_0(t), \qquad \sigma^f(0, t) = 0. \qquad [34]$$

For an "impermeable piston" the first component of the overall tension tensor and the equality of the rigid skeleton deformation and gaseous liquid are given as

$$\sigma^f(0, t) - p_m(0, t) - p_0 = \sigma_0(t), \qquad e_1 = e_m. \qquad [35]$$

This method of solution of [23, 24] with due account of boundary conditions [34] and [35] was realized by a computer, and a comparison of the calculated results with the experimental data is given below. Note that the propagation of pressure waves in a liquid-saturated porous medium can be described also by a linear system [23, 24]. For this we substitute p_2 instead of p_m, ρ_2 instead of ρ_m and K_2 instead of K_m in the coefficients H, M, C and D.

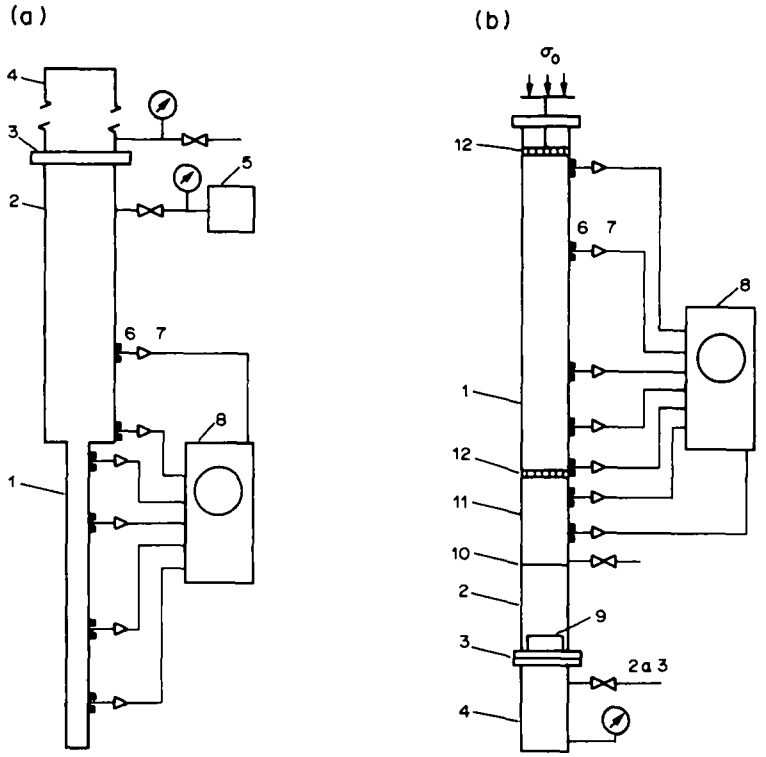

Figure 1. Schematic diagrams of the setup.

3. EXPERIMENTAL PROCEDURE

Experimental investigations of the propagation of pressure perturbations in porous media were carried out in two shock-tube setups (figure 1). Figure 1(a) represents the principal scheme of the setup for investigation of pressure wave propagation in consolidated liquid-saturated and gas bubble liquid-saturated porous media. The working section (1), which is a vertical thick-walled steel tube with i.d. 0.01 m and length 0.54 m, was filled with porous medium. Between the porous medium and working section wall a fluoroplastic $3 \cdot 10^{-6}$ m thick film was placed to eliminate the effects of porous medium friction against the walls of the working section on the wave propagation process. Chaotic packing made of plexiglass spheres, with dia $(0.2\text{–}0.25) \cdot 10^{-3}$ m, sintered just in the working section was used as the porous medium. Before the saturation with liquid the air was withdrawn from the working section by a pump (5) to prevent the appearance of air bubbles in the porous medium on its saturation with liquid. Benzine, kerosene and oil with differing viscosity, density and compressibility were used as working fluids. A porous medium saturated with liquid containing gas bubbles was generated in the following way. The liquid porous medium to be saturated was displaced equally by gas to the residual saturation of liquid distributed over the working section volume. Refilling of the working section was carried out at its continuous consumption rate which determined the residual void fraction in the range $0.01 < \epsilon_0 < 0.1$. To decrease the void fraction in the experiments, the static pressure p_0 in the working section was increased and the initial void fraction $\epsilon_0 = \epsilon_0^a p_a / p_0$ was decreased in comparison with the void fraction ϵ_0^a at atmospheric pressure p_a. Average in length section of the void fraction ϵ_0^a was determined by the measured rise of the liquid level Δh in a measuring tube over the porous medium for a decrease in the initial pressure p_0 up to p_v:

$$\epsilon_0^a = \frac{p_v \Delta h S_h}{[\phi l S_e (p_0 - p_v)]} \qquad [36]$$

where l is the porous medium height, and S_h and S_e are sections of the measuring tube and porous medium, respectively. At void fraction $\epsilon_0 < 0.01$, the gas phase in the liquid-saturated porous medium is in the form of gas bubbles. Uniform bubble distribution along the porous medium length was maintained by the velocity of the pressure perturbation propagation.

Two types of pressure wave propagation were studied experimentally. There are both step waves and bell-shape waves. Profiles of step pressure waves were generated by spontaneous rupture of a diaphragm (3) which divides low- (2) and high- (4) pressure chambers. At incidence of an air shock wave formed in a low-pressure chamber on a porous medium interface, there appears in the liquid a pressure equal to that in the reflected air wave, and the "liquid piston" boundary condition is realized. Bell-shape pressure pulse with an intensity of 0.1–1 MPa were caused by piston impact against a thin liquid layer above the porous medium or directly across the porous medium. In this case the "liquid piston" and "impermeable piston" boundary conditions, respectively, are realized.

Figure 1(b) shows the schematic diagram of the setup for investigation of bell-shape pressure pulse propagation, for intensities up to 25 MPa, in an unconsolidated liquid-saturated porous medium. The characteristic feature of the setup is the ability to obtain pressure pulses for a wide range of changing wave duration and amplitude at piston impact against the movable bottom (10) of a wave transformation chamber (11) filled with liquid. Piston acceleration occurs in the low-pressure chamber (2) under the influence of pressure drop, caused by diaphragm rupture. Pressure waves are generated in the wave transformation chamber and then propagate into the working section (1) filled with porous medium. The transformation chamber and working section are made of a thick-walled tube with i.d. $53 \cdot 10^{-3}$ m and wall thickness 8 mm. This allows exclusion of the effects of wall elasticity on the wave propagation process.

Unconsolidated river sand with particle dia $(0.01–0.5) \cdot 10^{-3}$ m refined from clay and organic admixtures was used as the porous medium. The method of wet stuffing was used to fill the working section with the medium. Sand was slowly poured with liquid into a reservoir and thoroughly mixed to exclude air bubbles. After this, liquid-saturated sand was poured into the working section, subjected to vibration and reduced by highly-permeable porous plates (12). This method allowed us to keep the medium porosity in the experiments constant. The modulus value of the volumetric skeleton elasticity K_B varied with the change at reduction of the degree of the porous skeleton at exterior loading σ_0. To control equilibrium loading along the length of the skeleton at reduction the working section was subjected to vibration. The value K_B was determined by the velocity of the compression wave propagation in the dry filling, taking into account the modulus of the rigid skeleton shift μ vs K_B (Domenico 1977):

$$\mu = 1.1 \cdot K_B. \qquad [37]$$

Wave profiles were measured by piezoelectric pressure transducers (6) (the diameter of the sensitive element being $2 \cdot 10^{-3}$ m) placed along the working section. The sensitive elements were not in contract with the porous medium skeleton and measured pressure in the liquid phase. Output signals, after passing through a high-resistance amplifier, were recorded with the help of an oscillograph (8).

4. EXPERIMENTAL RESULTS AND NUMERICAL CALCULATIONS

4.1. Pressure waves in consolidated liquid-saturated media

Figure 2 presents the calculated phase velocity $c_p = \mathrm{Re}(\omega/K)$ and attenuation coefficient $\eta_p = J_m K(\omega)$ vs frequency [28] for the parameters of the consolidated porous medium [sintered plexiglass liquid-saturated spheres (beads)] corresponding to the experimental conditions. As shown in figure 2, a "quick" wave propagates almost without dispersion and attenuation, but the "slow" wave has strong attenuation caused by the interphase friction on the liquid–rigid skeleton interface. Stoll (1980) showed that the character of the "quick" wave evolution substantially depends on the viscous elastic forces caused by the squeezing out of the liquid near the contact points of beads at their deformation. In view of these forces, the effective tension σ^f depends on the velocity of the rigid skeleton deformation. For harmonic waves this is equal to the substitution of the elastic coefficient H by the complex operator H^* into the system [23, 24] and, consequently, into the dispersion relation [28], which has the form

$$H^* = H + i\omega\beta_0 v\rho_2. \qquad [38]$$

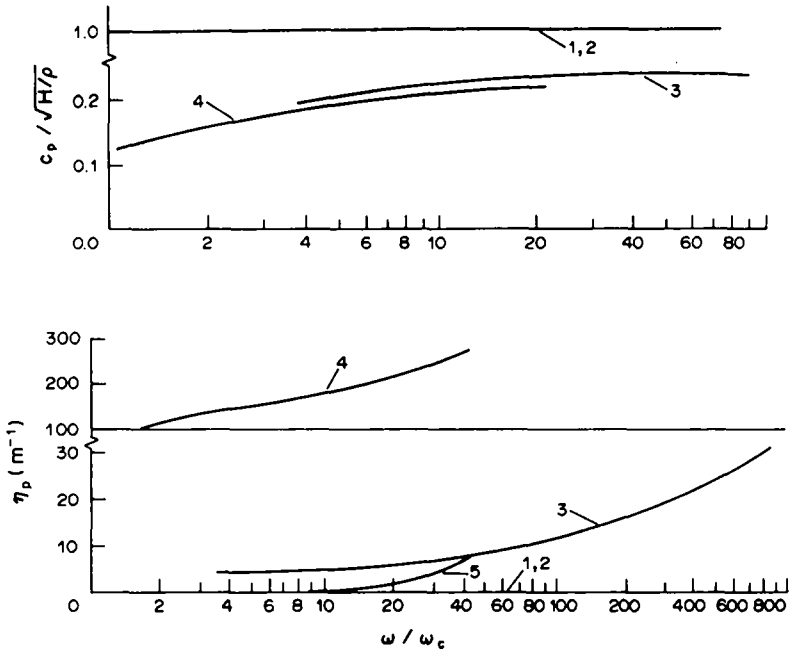

Figure 2. Calculated phase velocity and attenuation coefficient vs frequency for a consolidated liquid-saturated porous medium. (1, 3) Benzine; (2, 4, 5) oil; (1, 2) "quick wave" wave; (3, 4) "slow" wave; (5) "quick" wave with viscous elastic forces by [38].

Here β_0 is a coefficient depending on bead size and shape near the contact points, as well as the type of packing. For cubic packing of spherical particles with diameter d at their minimum approach at the distance h, Stoll (1980) obtained the following for β_0:

$$\beta_0 = \frac{d}{2h}. \qquad [39]$$

The value β_0 grows with an increasing number of bead contacts and, consequently, with packing density. The calculation of "quick" wave attenuation, with due account of viscous elastic forces according to [38], for an oil-saturated porous medium is presented in figure 2 (line 5 at $\beta_0 = 4 \cdot 10^3$). It is seen that dissipation, due to viscous elastic forces at high frequencies $\omega/\omega_c > 10$, will substantially influence the "quick" wave evolution.

Figure 3 shows experimental data (1) and calculated results (2) for the evolution of the pressure step profile with initial amplitude Δp_0 in a porous medium of sintered plexiglass beads saturated with benzine (a) and oil (b). It is seen that two types of longitudinal waves, "quick" and "slow" (Dontsov 1985; Dontsov *et al.* 1985) propagate in such media. The parameters of the consolidated porous medium are: $\phi = 0.35$; $K_0 = 18 \cdot 10^{-12}$ m^2; $K_B = 1.2 \cdot 10^9$ N/m^2; $\mu = 0.41 \cdot K_B$; $\rho_1 = 1.18 \cdot 10^3$ kg/m^3; $K_1 = 5.8 \cdot 10^9$ N/m^2; $\alpha = 3$. The moduli of the volumetric elasticity and porous skeleton shift were calculated by measuring the longitudinal wave velocity in a rod and in a plate made of sintered plexiglass beads. As the propagation velocity of a "quick" wave v_1 is essentially greater than that of a "slow" wave v_2, then already at the distance $x = 0.136$ m the division of the wave into a "quick" one and a "slow" one is observed [figure 3(a)]. As a result of dissipative processes on the interface, the "slow" wave front flattens substantially. With the increase in liquid viscosity the process of flattening also increases, and for highly viscous liquids it is almost impossible to detect the "slow" wave due to its immediate attenuation after division of the initial wave [figure 3(b)]. Even for viscous liquids the "quick" wave maintains its shape almost constant at the distances studied.

Calculated results via a linear model [23, 24] describe rather well the generation of "quick" (with amplitude Δp_{10}) and "slow" (with amplitude Δp_{20}) waves from an initial signal Δp_0 and their evolution along the length of the working section. Oscillations of waves on the second and third

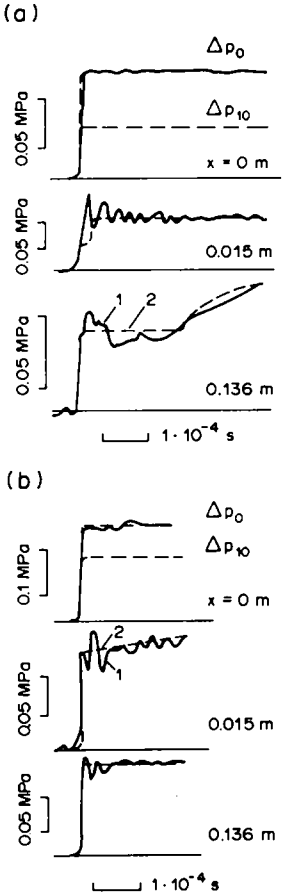

Figure 3. Evolution of the stepwise pressure profile in a consolidated liquid-saturated porous medium. (1) Experiment; (2) calculation by model [23, 24]. (a) Benzine—$\rho_2 = 0.75 \cdot 10^3$ kg/m^3, $K_2 = 0.86 \cdot 10^9$ N/m^2, $\nu = 0.72 \cdot 10^{-6}$ m^2/s. (b) Oil—$\rho_2 = 0.86 \cdot 10^3$ kg/m^3, $K_2 = 1.51 \cdot 10^9$ N/m^2, $\nu = 25.2 \cdot 10^{-6}$ m^2/s.

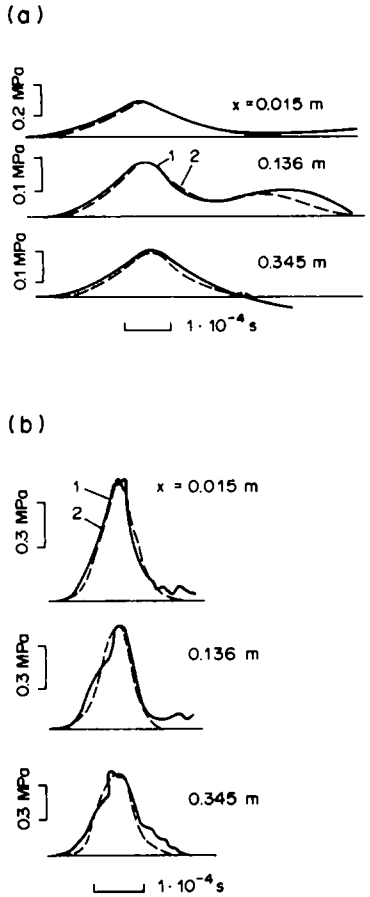

Figure 4. Evolution of a bell-shape pressure wave. (1) Experiment; (2) calculation by model [23, 24]; (a) "Liquid piston"; (b) "impermeable piston".

transducers are caused by the peculiarities of air shock wave entry into the liquid-saturated porous medium.

Figure 4 represents profiles of bell-shape pressure waves (1) in comparison with calculations (2) at different distances from entry into a benzine-saturated porous medium. The medium parameters correspond to the parameters in figure 3(a). The pressure wave profiles in figure 4(a, b) correspond to different types of wave perturbations, i.e. "liquid piston" and "impermeable piston", respectively. As for the step pressure profile at the "liquid piston" boundary condition [figure 4(a)], two waves ("quick" and "slow") are generated from the initial signal at the distance $x = 0.136$ m. The "quick" wave does not attenuate in the range of wave and medium parameters studied, but the attenuation of the "slow" wave is significant. This difference is caused by the fact that in the "quick" wave the shifts of the liquid and rigid skeleton are almost equal in size and coincide in phase, but in the "slow" wave these shifts occur in counter-phase (Biot 1956).

In contrast to the "liquid piston", the total initial signal generates a "quick" wave at the "impermeable piston" but a "slow" wave is not observed, even for a porous medium saturated with a low-viscous liquid (benzine) [figure 4(b)].

The coefficient of added mass α varied in the calculations. The best correlation of the experimental data with the calculated results for wave division, attenuation and propagation velocity was observed at $\alpha = 3$. The value of α essentially influences the propagation velocity and attenuation intensity of the "slow" wave, but the "quick" wave evolution in a consolidated phase is almost independent of α.

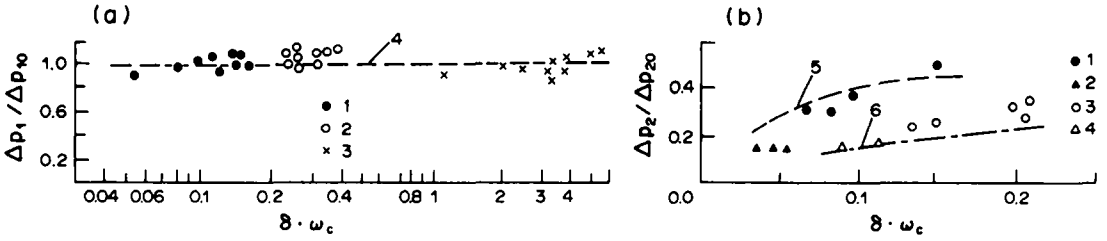

Figure 5. Attenuation of a bell-shape presure wave vs its duration. (a) "Quick" wave, experiment: (1) benzine; (2) kerosene; (3) oil; (4) calculation by [23, 24]. (b) "slow" wave, experiment: (1, 2) benzine; (3, 4) kerosene; (1, 3) $\Delta p_{20} = 0.1$–0.3 MPa; (2, 4) $\Delta p_{20} = 0.6$–0.8 MPa; (5, 6) calculations for benzine and kerosene, respectively.

Note that in the calculations the initial bell-shape signal was approximated by the relation

$$\Delta p(t) = \Delta p_0 \exp\left[-\left(\frac{2t}{\delta}\right)^2\right], \qquad [40]$$

where δ is the signal duration at the level $0.37 \cdot \Delta p_0$.

Experimental data on the attenuation of "quick" (a) and "slow" (b) wave amplitudes for different durations of the signal entering the medium are shown in figure 5. Here Δp_1 and Δp_2 are the wave amplitudes at the distance $x = 0.136$ m from the medium input; Δp_{10} and Δp_{20} are "quick" and "slow" wave amplitudes at the medium input, respectively. The physical properties of kerosene are: $\rho_2 = 0.8 \cdot 10^3$ kg/m^3; $\nu = 1.7 \cdot 10^{-6}$ m^2/s; $K_2 = 1.2 \cdot 10^9$ N/m^2; other medium parameters correspond to those in figure 3. In the range of wave duration and medium parameters studied, the "quick" wave does not attenuate, which corresponds with our calculations (4) [figure 5(a)]. For the "slow" wave, amplitude attentuation vs wave duration was observed in the experiments [figure 5(b)]. The "slow" wave amplitude at the medium input Δp_{20} was calculated by the measured "quick" wave amplitude, with the help of the calculated value for the "quick" wave amplitude vs the "slow" wave amplitude at the medium input. The calculated curves for benzine (5) and kerosene (6) give good correlations for the experimental data for wave amplitudes < 0.3 MPa. At greater amplitudes, for the benzine-saturated porous medium greater attenuation is observed than the calculations predict. This seems to be caused by a divergence in liquid flow behind the wave, given by Darcy's law with the increase in Re. So, for amplitudes $\Delta p_{20} = 0.6$–0.8 MPa, Re is equal to 30–40, which gives a correction to the interphase friction due to the nonlinear term in Forchheimer's law ($\sim 40\%$), Re is determined by the liquid velocity vs the rigid skeleton in wave Δu and bead diameter d.

As shown in figure 2, the "quick" wave evolution at high frequencies is significantly influenced by viscous elastic forces caused by the squeezing out of viscous liquid near the contact points of the solid particles at their deformation. Figure 6 presents the evolution character of a stepwise "quick" wave front in an oil-saturated porous medium. The medium parameters correspond to those in figure 3(b). For a steep wave front a pronounced flattening of the wave profile is observed.

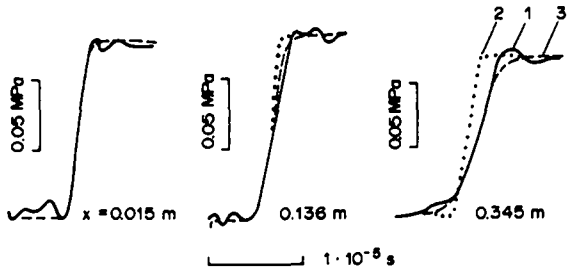

Figure 6. Front structure of a stepwise "quick" wave in an oil-saturated porous medium. (1) Experiment; (2) calculation by [23, 24]; (3) calculation with [38].

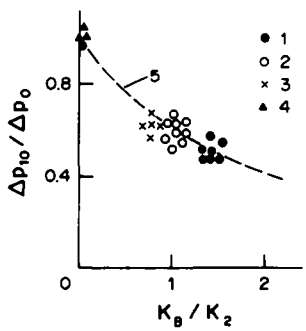

Figure 7. Dependence of the "quick" wave amplitude at input into a porous medium at generation from the initial signal on the moduli of the volumetric elasticity of the porous skeleton vs liquid. Experiment: (1) benzine; (2) kerosene; (3, 4) oil; (5) calculation by [23, 24].

Comparison with the calculations (2) via [23, 24] shows that the front flattening in the experiment is more severe (this can be accounted for by neglecting viscous elastic forces). Introduction of the complex modulus H^* by [38] allows us to describe the wave structure more precisely (line 3). The best agreement with the experiments was observed at the coefficient value $\beta_0 = 4 \cdot 10^3$. For the sand liquid-saturated porous medium, as shown by Stoll (1980), the coefficient β_0 changes in the range 10^4–10^5. Note that for the experimental data shown in figure 5 the influence of viscous elastic forces is very small and is seen in signals of significantly shorter duration or at large distances from the porous medium input.

The amplitudes of "quick" and "slow" waves at the porous medium input are determined by the conditions of the wave perturbation and the medium parameters. Figure 7 presents experimental data for the "quick" wave amplitude at the porous medium input at the generation from the initial signal vs the relation K_B/K_2 at the "liquid piston" boundary condition. The medium parameters for experimental data plots 1–3 correspond to those in figures 3 and 5, and for experimental data plot 4, $K_B = 0.05 \cdot 10^9$ N/m^2. Here the calculated results for all three types of liquid, which also coincide (line 5), are also presented. The calculated result show that the "quick" wave amplitude under the given experimental conditions depends slightly on the liquid viscosity and density, and is determined, mostly, by the value K_B/K_2 for the given skeleton material.

Figure 8 presents the experimental data concerning the propagation velocity of "quick" v_1 and "slow" v_2 waves vs their amplitudes. In the range of wave intensity studied the velocities of "quick" [figure 8(a)] and "slow" [figure 8(b)] waves are independent of their amplitudes and coincide with

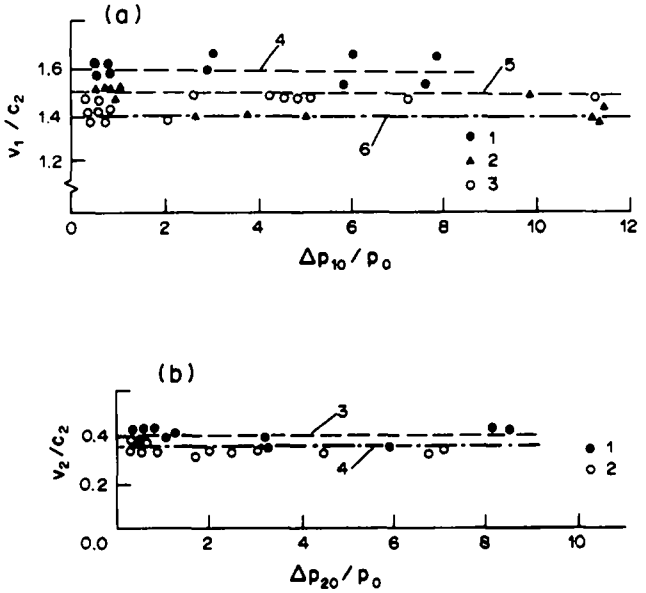

Figure 8. Velocity of pressure wave propagations vs their amplitudes. (a) "Quick" wave: (1, 2, 3) experiment; (4, 5, 6) calculation by [23, 24]; (1, 4) benzine; (2, 5) kerosene; (3, 6) oil. (b) "Slow" wave: (1, 2) experiment; (3, 4) calculation by [23, 24]; (1, 2) benzine; (3, 4) kerosene. $p_0 \approx 0.1$ MPa.

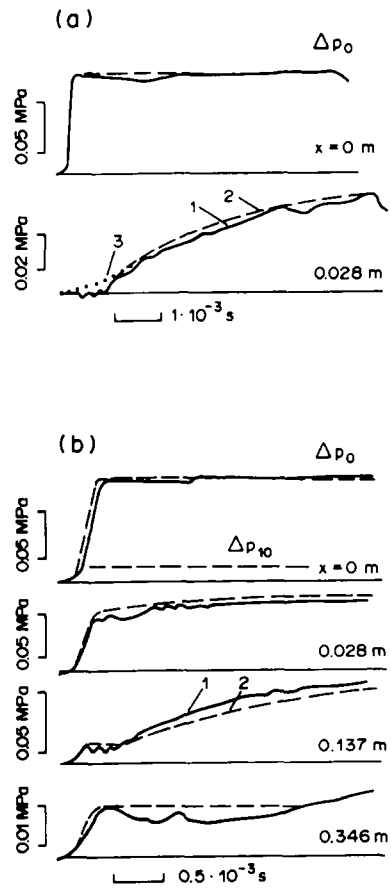

Figure 9. Evolution of a stepwise profile pressure wave in a consolidated porous medium saturated by kerosene with air bubbles. (1) Experiment; (2) calculation by [23, 24]; (3) calculation by [41]. (a) $\epsilon_0 = 2.6\%$, $p_0 = 0.1$ MPa. (b) $\epsilon_0 = 0.24\%$, $p_0 = 0.3$ MPa.

the calculated values. This proves the validity of using the linear equation set [23, 24] for the analysis of the wave propagation process in the amplitude range studied.

4.2. Pressure waves in a consolidated porous medium saturated with liquid with gas bubbles

The results of the experiments show that in a consolidated porous medium saturated with gas bubbles and liquid two types of longitudinal waves, "quick" and "slow", also propagate. In figure 9 the evolution character of the stepwise pressure profile in a porous medium consisting of sintered plexiglass spheres and saturated with kerosene with gas bubbles at different p_0 and ϵ_0 is shown. The parameters of the porous skeleton and saturating liquid ($\phi = 0.35$; $K_0 = 18 \cdot 10^{-12}$ m^2; $K_B = 1.2 \cdot 10^9$ N/m^2; $\mu = 0.41 \cdot K_B$; $\alpha = 3$; $\rho_2 = 0.81 \cdot 10^3$ kg/m^3; $\nu = 1.7 \cdot 10^{-6}$ m^2/s; $K_2 = 1.2 \cdot 10^9$ N/m^2) remained constant for all the experiments described.

At large volumetric void fractions ($\epsilon_0 \sim 1$–5%) and the initial atmospheric pressure ($p_0 = 0.1$ MPa) the "quick" wave is almost not generated [figure 9(a)]. With the decrease of ϵ_0 and an increase in p_0, the "quick" wave amplitude increases [figure 9(b)]. In all the perturbation and medium ranges studied the severe flattening of the "slow" wave front caused by the interphase friction effect on the wave evolution process was observed. With the increase in volumetric void fraction the process of wave-front flattening becomes more severe. The "quick" wave amplitude and steepness of its front change slightly along the working section. The "quick" wave velocity is determined, mostly, by the compressibility of the porous skeleton and depends slightly on the value of the volumetric void fraction in the range studied, $0.2 \lesssim \epsilon_0 \lesssim 2\%$.

With the increase in the initial static pressure the steepness of the wave front at the porous medium interface decreases as a result of flattening of the air wave front, and typical wave frequencies are much lower than the resonant frequency of bubble oscillation. In this case waves of small amplitude, as shown in section 2, will be described by system [23, 24]. The solution of pressure wave profiles by this equation set made for the "liquid piston" boundary condition and initial medium parameters corresponding to the given experimental conditions, is shown by line 2 in figure 9. The calculation results describe well the initial "quick" and "slow" wave amplitudes at generation from the initial signal vs their evolution along the working section length x. Processing of the experimental data for the "quick" wave velocity shows that in the range of measurement accuracy the velocity value $v_1 = 1.4 \cdot 10^3$ m/s, for wave intensities $\Delta p_{10}/\Delta p_0 \lesssim 0.05$, coincides with the calculated value $v_{1c} = 1.45 \cdot 10^3$ m/s. The "slow" wave velocity, due to its strong attenuation, was ignored.

Note that in the calculations the value of 1 was substituted for that of adiabatic γ in the set [23, 24], because the time for thermal gas relaxation in a bubble $\tau_0 = R_0^2/\pi^2 a$ is much less than the time of pressure growth in a wave front and the process of compressibility of a bubble in a wave is isothermal; a is the gas temperature conductivity in a bubble. The air bubble diameter in a porous medium for small volumetric void fractions $\epsilon_0 \lesssim 1\%$ is almost the same as the maximum pore size in such a medium (Wardlaw & Kellar 1985). Using for the evaluation of bubble radius a porous medium with cubic packing of equal-sized spheres, in which the maximum pore size is $0.7d$ (d is the sphere diameter), one obtains for the experiments $R_0 \sim 0.7 \cdot 10^{-4}$ m.

The experimental data and theoretical results for the "quick" wave amplitude at input into a porous medium at generation from the initial signal vs the relation between the moduli of the volumetric skeleton elasticity and the gas–liquid mixture are shown in figure 10. With the increase in K_B/K_m, that corresponds to the increase in the volumetric void fraction ϵ_0, the "quick" wave amplitude significantly decrease and at $p_0 = 0.1$ MPa and $\epsilon_0 = 1\%$ almost the entire initial wave transforms into a "slow" one. So, due to the strong attenuation of the "slow" wave and essentially nonequilibrium division of the input wave into a "quick" and a "slow" one, at $\epsilon_0 > 1\%$ the pressure perturbation at the medium input attenuates almost completely at a distance of a few wavelengths. The numerical calculations of the wave evolution at the medium input describe rather well the experimental data for the wave intensity range studied, $\Delta p_0/p_1 < 1$.

As shown by Chandler & Johnson (1981), the set of equations [23, 24] for low-frequency "slow" waves can be reduced to one equation of diffusion type. The solution of this equation for the initial stepwise signal has the form:

$$\Delta p_2(x, t) = \Delta p_{20} \operatorname{erfc}\left(\frac{x}{2\sqrt{a_0 t}}\right), \qquad [41]$$

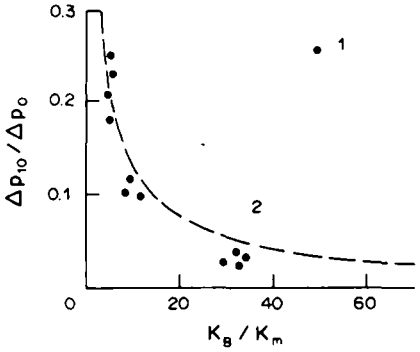

Figure 10. "Quick" wave amplitude at input into the porous medium at generation from the initial signal vs K_B/K_m. (1) Experiment; (2) calculation by [23, 24].

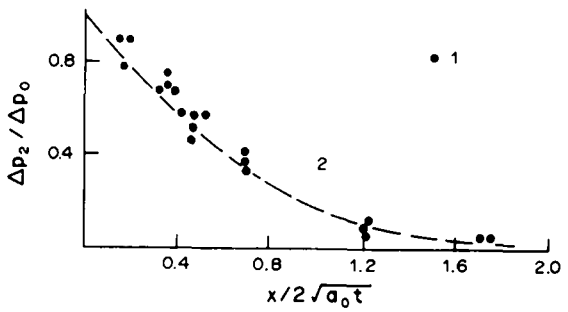

Figure 11. "Slow" wave attenuation. (1) Experiment; (2) calculation by [41]. $p_0 = 0.1$ MPa, $\Delta p_0/p_0 \lesssim 2$, $\epsilon_0 \gtrsim 0.5\%$.

where $a_0 = c_0^2 K_0/\phi v$. Calculation of profile by [41] is shown in figure 9 (line 3). Unlike the exact solution by [23, 24], solution [41] yields an infinite propagation velocity but describes the "slow" wave profile well, except for the initial part of its front.

Correlation of the experimental data on the attenuation of the pressure in a stepwise profile wave of duration $t_0 = 5.5 \cdot 10^{-3}$ s with the calculated results by [41] is shown in figure 11. Thus, experimental data on "slow" wave attenuation at $\epsilon_0 \gtrsim 0.5\%$ can be well-described with the help of the approximate calculation [41].

With the increase in wave amplitude the nonlinearity of the medium begins to influence the "slow" wave evolution. Figure 12 presents the experimental data on the pressure maximum in a "slow" wave of duration $t_0 = 5.5 \cdot 10^{-3}$ s at a small distance x from the medium input vs the initial signal amplitude. For $\Delta p_0/p_0 \gtrsim 5$, the contribution of the nonlinear effects to the wave attenuation becomes significant, and for a precise description of the "slow" wave evolution it is necessary to solve the equation set [19, 20, 22], where the nonlinearity caused by the gas bubbles is taken into account.

Unlike "slow" waves, in "quick" waves the dissipative losses and nonlinear effects conditioned by bubble pulsation in the water manifest themselves at essentially small wave amplitudes. For a rather strong stepwise wave with a steep front, nonlinearity leads, as in gas bubble liquid, to the possibility of an oscillating wave structure (figure 13). In front of the wave, as in a gas bubble liquid (Kuznetsov & Pokusayev, 1978), the forerunner propagates. The wave relaxation zone seems to be determined by the interphase friction on the liquid–rigid skeleton interface and the equalization of temperature in the liquid and gas. The wave front oscillation frequency is almost equal to the bubble oscillation resonant frequency. For the description of oscillation wave structures numerical calculations via the set [19, 20, 22] are necessary.

4.3. Pressure waves in an unconsolidated liquid-saturated porous medium

The experimental results show that in unconsolidated liquid-saturated sand, with the modulus of the volumetric skeleton elasticity less than that of the liquid, only one longitudinal wave propagates at a velocity v_1 almost equal to the speed of sound in the liquid (Dontsov 1985; Dontsov *et al.* 1985). Line 1 in figure 14 shows the character of the pressure wave evolution in oil-saturated

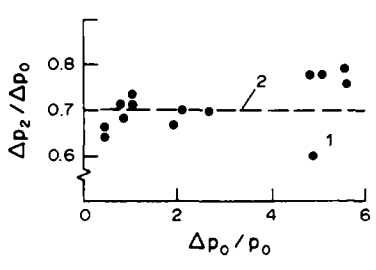

Figure 12. "Slow" wave attenuation vs its intensity at the porous medium input. (1) Experiment; (2) calculation by [23, 24]. $x = 0.028$ m, $p_0 = 0.1$ MPa, $\epsilon_0 = 0.7\%$.

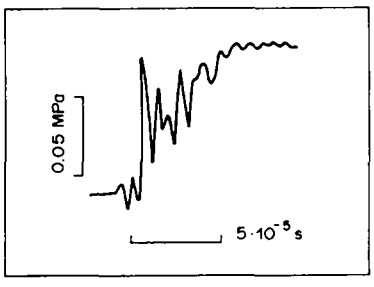

Figure 13. Oscillating structure of a "quick" pressure wave front. $x = 0.137$ m, $p_0 = 0.3$ MPa, $\epsilon_0 = 0.36\%$.

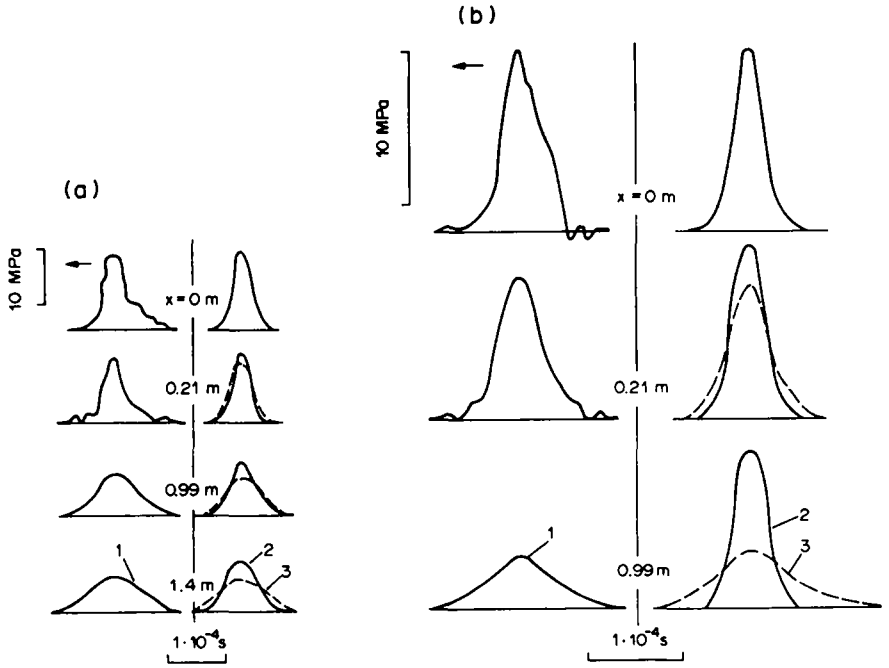

Figure 14. Evolution of a bell-shape pressure wave in unconsolidated oil-saturated sand. (1) Experiment; (2) calculation by [23, 24]; (3) calculation by [43]. $K_{BI}/K_B = 0.5$, $\mu_1/\mu = 0.5$, $\rho_2 = 0.86 \cdot 10^3$ kg/m^3, $K_2 = 1.25 \cdot 10^9$ N/m^2, $\nu = 32.4 \cdot 10^{-6}$ m^2/s. (a) $K_B = 10^8$ N/m^2, $\phi = 0.33$, $K_0 = 24 \cdot 10^{-12}$ m^2, $v_1 = 1.39 \cdot 10^3$ m/s, $v_{1c} = 1.39 \cdot 10^3$ m/s. (b) $K_B = 0.5 \cdot 10^9$ N/m^2, $\phi = 0.30$, $K_0 = 16 \cdot 10^{-12}$ m^2, $v_1 = 1.59 \cdot 10^3$ m/s, $v_{1c} = 1.58 \cdot 10^3$ m/s.

unconsolidated sand for different medium parameters. At $x = 0$, pressure wave profile in the porous medium at a distance of 0.012 m from the medium input was considered to be the initial signal. The parameters of the porous skeleton material are $\rho_1 = 2.56 \cdot 10^3$ kg/m^3 and $K_1 = 4 \cdot 10^{10}$ N/m^2. It is clear that at wave propagation its amplitude decreases and its duration grows. By comparison of the wave amplitudes in figures 14(a) and (b), we determine that with the increase in the modulus of the volumetric skeleton elasticity K_B, the wave attenuation increase in the input signal duration leads to a decrease in attenuation, and that a change in the viscosity of the liquid which saturates the medium by 20 fold is not important for wave evolution.

Line 2 in figure 14 shows the results calculated by the system [23, 24]. The initial signal was approximated by [40]. The value of the added liquid mass affected the wave evolution slightly and was calculated by the Berryman (1981) formula:

$$\alpha = 1 - \frac{1}{2} \cdot \left(1 - \frac{1}{\phi}\right). \qquad [42]$$

This corresponds to the data of Domenico (1977) for unconsolidated sand at weak reduction. The calculated results proved that at $K_B \ll K_2$ in a porous liquid-saturated medium only one longitudinal wave, i.e. the "quick" one, propagates. Comparison of the experimental and calculated results shows that attenuation in the experiments is greater than that in the calculations. In addition, the increase in K_B in the experiments leads to an increase in wave attenuation, but in the calculations this increase leads to a decrease in attenuation. This means that, in contrast to a consolidated porous medium, in an unconsolidated medium there exists, besides the interphase friction which is taken into account in the Biot (1956) theoretical model, an additional mechanism of dissipation.

As shown by Stoll (1977), at pressure wave propagation in an unconsolidated porous medium shifts of the solid particles and losses due to friction between the particles are possible. This leads to the appearance of "dry" friction forces, which at low frequencies predominate over interphase friction forces. "Dry" friction for harmonic waves can be taken into account by substitution of the complex moduli of the volumetric elasticity $\bar{K}_B$ and the porous skeleton shift $\bar{\mu}$, instead of their real values K_B and μ, into the equation set [23, 24]:

$$\bar{K}_B = K_B + iK_{BI}, \qquad \bar{\mu} = \mu + i\mu_1. \qquad [43]$$

Hall & Richart (1963) have shown that imaginary modulus parts vs real ones, K_{BI}/K_B and μ_I/μ, slightly increase with the growth of skeleton elasticity e_1 and, for $10^{-5} < e_1 < 10^{-4}$, they change in the interval 0.03–0.07. Comparison of the calculated results after introduction of the complex moduli with the experimental data showed good correlation for $K_{BI}/K_B = 0.5$ and $\mu_I/\mu = 0.5$ (figure 14). For the presented experimental data the value $e_1 \sim 10^{-2}$ caused the increase in K_{BI}/K_B and μ_I/μ, in comparison with the data obtained by Hall & Richart (1963). The deformation value was evaluated by the relation $e_1 \sim \Delta p_0 \phi / K_2$.

The measured values of the wave velocity v_1 in figure 14 coincide with the calculated values v_{1c} within measurement error. Note that introduction of the complex moduli is not important for wave velocity. Comparison of the experimental results with the calculations showed that the "quick" wave propagation velocity and its degree of attenuation were almost independent of the coefficient of added liquid mass α.

For low frequencies of the process $\omega < \omega_c = \phi v / 20 K_0$ and at $K_B < K_2 < K_1$ and substituting $\bar{K}_B$ and μ, instead of the real modulus values K_B and μ, and with "dry" friction between the porous medium particles in [28] (for a porous liquid-saturated medium), we obtain the equations for the propagation velocity v_1 and attenuation coefficient K_1 of harmonic waves:

$$v_1 = \left(\frac{H}{\rho_0}\right)^{1:2} \qquad [44]$$

and

$$K_1 = \ln \frac{\left(\frac{\Delta p_0}{p_0}\right)}{x} = \alpha_v + \alpha_1, \qquad [45]$$

where

$$\alpha_v = \frac{K_0 \omega^2 (\rho_0 - \rho_{20})^2}{2 v v_1 \rho_0 \rho_{20}} \qquad [46]$$

and

$$\alpha_1 = \frac{(K_{BI} + \frac{4}{3}\mu_1)\omega}{2v1\left(\frac{K_2}{\phi} + \frac{4}{3}\mu + K_B\right)}. \qquad [47]$$

The coefficient α_v is determined by dissipative losses at the phase interface and α_1 is determined by the "dry" friction between the porous medium particles. For frequencies

$$\omega \ll \frac{\rho_0 \rho_{20} \nu (K_{BI} + \frac{4}{3}\mu_1)}{K_0(\rho_0 - \rho_{20})^2 \left(\frac{K_2}{\phi} + K_B + \frac{4}{3}\mu\right)}$$

we can neglect the dissipitation on the phase interface, and the attenuation coefficient is of the form

$$K_1 = \alpha_1 \sim \omega. \qquad [48]$$

The linear attenuation coefficient vs frequency can be used for correlation of the experimental data for pressure pulse attenuation by the transition from the typical pulse duration δ to its typical frequency $\omega^* = 1/\delta$.

The experimental data on the attenuation of bell-shape pressure waves in unconsolidated sand (with $K_B = 0.5 \cdot 10^9$ N/m^2) saturated with liquid for different wave durations δ, wave amplitudes Δp_0 and liquid viscosity ν are given in figure 15, where

$$\bar{\alpha} = \frac{K_{BI} + \frac{4}{3}\mu_1}{2 v_1 \delta \left(\frac{K_2}{\phi} + K_B + \frac{4}{3}\mu\right)}.$$

The oil parameters correspond to those in figure 8, and the kerosene parameters are $\rho_2 = 0.79 \cdot 10^3$ kg/m^3, $K_2 = 0.9 \cdot 10^9$ N/m^2 and $\nu = 1.54 \cdot 10^{-6}$ m^2/s.

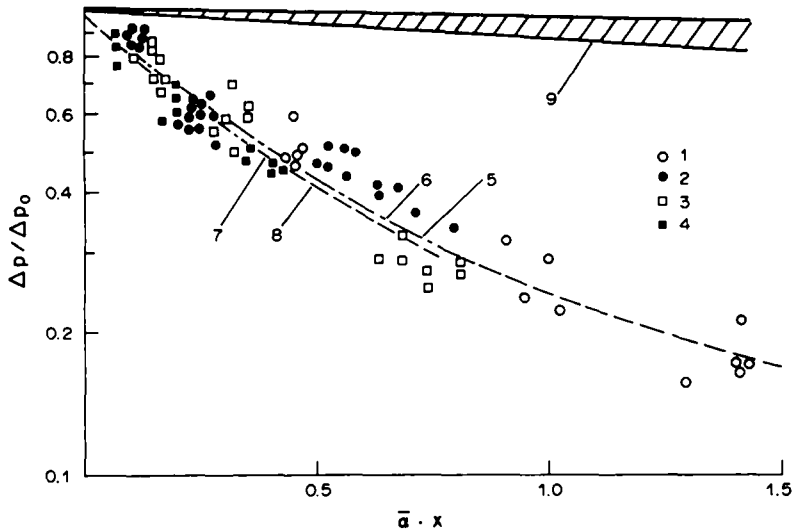

Figure 15. Attenuation of a bell-shape pressure wave in liquid-saturated sand. $K_B = 0.5 \cdot 10^9$ N/m^2, $\phi = 0.30$, $K_0 = 16 \cdot 10^{-12}$ m^2. Experiment: (1, 2) kerosene; (3, 4) oil; (1, 3) $\delta = (45\text{–}55) \cdot 10^{-6}$ s, $\Delta p_0 = 7\text{–}25$ MPa; (2, 4) $\delta = (80\text{–}100) \cdot 10^{-6}$ s, $\Delta p_0 = 2\text{–}5$ MPa. Calculation by [23, 24] with "dry" friction [43], $K_{BI}/K_B = 0.5$, $\mu_1/\mu = 0.5$: (5, 6) kerosene, (7, 8) oil, (5, 7) $\delta = 48 \cdot 10^{-6}$ s; (6, 8) $\delta = 10^{-4}$ s. (9) Calculation by [23, 24].

Also given in figure 15 are the calculated results of the wave amplitudes at different distances x from the porous medium input. Calculations 5–8 are presented with "dry" friction and dissipation at the phase interface. The experimental data are well correlated with the calculated results, and almost coincide for different perturbation and medium parameters in dimensionless coordinates. This is due to the weak influence of the phase interface dissipation on the wave amplitude attenuation. The calculated results without "dry" friction for all wave and medium parameters lie in the region 9 and yield essentially smaller attenuation than the experimental data.

The deviation of the calculated results 5–8 from the direct lines in the given coordinates is connected with the increase in wave duration at evolution along the working section, which leads to a decrease in typical wave frequencies and, correspondingly, to a decrease in the degree of attenuation.

The experimental data on pressure wave attenuation in an unconsolidated porous medium with the modulus of the volumetric skeleton elasticity $K_B = 10^8$ N/m^2 for different wave durations and intensities are shown in figure 16. Oil with the same parameters as those in figure 14 was used as the working liquid. It is clear that with the decrease in K_B, the role of dissipative processes at the phase interface grows which leads to a more pronounced disagreement between calculations 3 and 4 in dimensionless coordinates, taking into account only the "dry" friction.

In a recent paper McCann & McCann (1985) have shown that a linear dependence of attenuation on frequency, which is observed experimentally, can be obtained, taking into account both the "dry

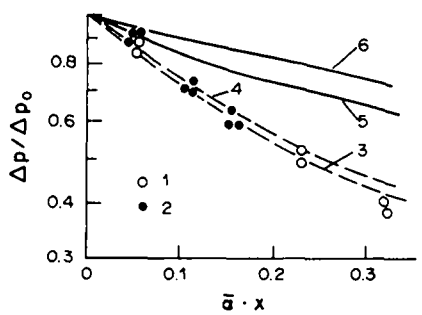

Figure 16. Pressure wave attenuation in oil-saturated sand. $K_B = 10^8$ N/m^2, $\phi = 0.33$, $K_0 = 24 \cdot 10^{-12}$ m^2: (1, 2) experiment; (3,. 4) calculation by [23, 24] with "dry" friction [43]. $K_{BI}/K_B = 0.5$, $\mu_1/\mu = 0.5$: (5, 6) calculation by [23, 24]; (1, 3, 5) $\delta = 48 \cdot 10^{-6}$ s; (2, 4, 6) $\delta = 10^{-4}$ s.

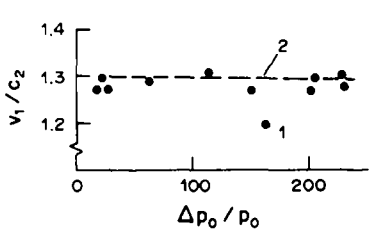

Figure 17. Wave velocity vs its intensity. $p_0 = 0.1$ MPa, $\delta \approx 48 \cdot 10^{-6}$ s. (1) Experiment; (2) calculation by [23, 24] with "dry" friction [43].

friction" of particles and including a pore size distribution into a modified Biot theory. At the same time, such an approach does not allow us to account for the increase in attenuation in pressure waves with the increase in external load on a porous medium (increase of the bulk modulus), which is observed experimentally at small variations of medium permeability (small variation of pore size distribution).

The comparison of the experimental data with calculation by wave velocity vs its initial intensity in oil-saturated sand is shown in figure 17. The medium parameters correspond to those in figure 14(b). The experimental data on the wave velocity are independent of the amplitude of the initial pressure perturbation and are in good agreement with the calculated value. The experimental data given in figure 17 prove the validity of the linear equation set [23, 24] for the description of pressure wave propagation in the amplitude range studied.

Acknowledgements—The authors acknowledge the assistance of Z. M. Orenbakh (Institute of Thermophysics, Novosibirsk) in compiling a program for numerical calculation by the fast Fourier transform method.

REFERENCES

ANDERSON, A. L. & HAMPTON, L. D. 1980 Acoustics of gas-bearing sediments. 1. Background. 2. Measurements models. *J. acoust. Soc. Am.* **67,** 1865–1903.

BEDFORD, A. & STERN, M. 1983 A model for propagation in gassy sediments. *J. acoust. Soc. Am.* **73,** 409–417.

BERRYMAN, J. G. 1981 Elastic wave propagation in fluid-saturated porous media. *J. acoust. Soc. Am.* **69,** 416–424.

BIOT, M. A. 1956 Theory of propagation of elastic waves in a fluid-saturated porous solid. *J. acoust. Soc. Am.* **28,** 168–191.

CHANDLER, R. N. & JOHNSON, D. L. 1981 The equivalence of quasistatic flow in fluid-saturated porous media and Biot's slow wave in the limit of zero frequency. *J. appl. Phys.* **52,** 3391–3395.

DOMENICO, S. M. 1977 Elastic properties of unconsolidated porous and reservoirs. *Geophysics* **42,** 1339–1368.

DONTSOV, V. E. 1985 Pressure wave propagation in liquid-saturated porous medium. In *Actual Problems of Thermophysics and Physical Hydrodynamics* (Edited by NAKORYAKOV, V. E.), pp. 59–65. Institute of Thermophysics, Novosibirsk.

DONTSOV, V. E., KUZNETSOV, V. V. & NAKORYAKOV, V. E. 1985 Pressure wave evolution in liquid-saturated porous medium. In *Abstr. IVth All-Union Symp. on Physics of Hydrodynamic Phenomena and Optical Acoustics*, Ashkhabad, p. 95.

HALL, J. R. & RICHART, F. E. 1963 Dissipation of elastic wave energy in granular soils. *J. Soil. Mech. Fdn Div. ASCE* **89,** 27–56.

HOVEM, J. M. & INGRAM, G. D. 1979 Viscous attenuation of sound in saturated sand. *J. acoust. Soc. Am.* **66,** 1807–1812.

JOHNSON, D. L. & PLONA, T. J. 1982 Acoustic slow wave and the consolidation transition. *J. acoust. Soc. Am.* **72,** 556–565.

KUZNETSOV, V. V. & POKUSAYEV, B. G. 1978 Pressure wave dynamics in liquid with gas bubbles. In *Transformation of the Laminar Boundary Layer into a Turbulent One* (Edited by KUTATELADZE, S. S.), pp. 61–67. Institute of Thermophysics, Novosibirsk.

LYAKOV, G. M. 1974 *Fundamentals of Explosion Wave Dynamics in Soil and Rocks.* Nauka, Moscow.

MCCANN, C. & MCCANN, D. M. 1985 A theory of compressional-wave attenuation in noncohesive sediments. *Geophysics* **50,** 1311–1317.

NAKORYAKOV, V. E., SOBOLEV, V. V. & SHREIBER, I. R. 1972 Long-wave perturbations in gas–liquid mixtures. *Izv. Akad. Nauk SSSR* **5,** 71–76.

NAKORYAKOV, V. E., POKUSAYEV, B. G. & SHREIBER, I. R. 1983 Wave propagation in gas- and vapour–liquid media. Institute of Thermophysics, Novosibirsk.

NIGMATULIN, R. I. 1978 *Fundamentals of Mechanics of Heterogeneous Media.* Nauka, Moscow.

NIKOLAYEVSKY, V. N., BASNIEV, K. S., GORBUNOV, A. T. & ZOTOV, G. A. 1970 *Mechanics of Saturated Porous Media.* Nauka, Moscow.

PLONA, T. J. 1980 Observation of a second bulk compressional wave in a porous medium at ultrasonic frequencies. *Appl. Phys. Lett.* **36,** 259–261.

SALIN, D. & SCHON, W. 1981 Acoustics of water saturated packed glass spheres. *J. Phys. Lett.* **42,** L477–L480.

STOLL, R. D. 1977 Acoustic waves in water-saturated sediments. In *Physics of Sound in Marine Sediments* (Edited by HAMPTON, L.). Nauka, Moscow.

STOLL, R. D. 1980 Theoretical aspects of sound transmission in sediments. *J. acoust. Soc. Am.* **68,** 1341–1350.

WARDLAW, N. C. & KELLAR, M. 1985 Oil blob populations and mobilization of trapped oil in unconsolidated packs. *Can. J. chem. Engng* **63,** 525–532.